Energy, Mines and Resources Canada | Énergie, Mines et Ressources Canada

CANMET

Canada Centre for Mineral and Energy Technology | Centre canadien de la technologie des minéraux et de l'énergie

IMAGE ANALYSIS STUDY OF SAMPLES FROM UNIVERSITY OF WALES, COLLEGE OF CARDIFF

R. Lastra and R. Pinard

Mineral Processing Laboratory

May 1990

MICROMEDIA

Project: 30.05.02
Mineralogical Evaluation of Process Products

24 pp

MINERAL SCIENCES LABORATORIES
DIVISION REPORT MSL 90-39 (IR)

This document is an unedited ... prepared primarily ... purpose. It does not ... final expression of ... division of the Canada Centre ... Mineral and Energy Technology (CANMET)

Ce document est un rapport ... rédigé principalement pour ... documentation ... ne ... finale ... de l'opinion du Centre canadien de la technologie des minéraux et de l'énergie (CANMET)

90-06002/

Image analysis study of samples from University of Wales, College of Cardiff

R. Lastra R. Pinard

March 17, 1990
Revised May 11, 1990
Project: 30.05.02
Division Report MSL 90-39 (IR)

Abstract

Samples from tests conducted by Dr. K.P. Williams on an EEC project were received to determine why the copper is slow floating.

The samples were studied using a Microprobe SEM-IPS image analysis system (MP-SEM-IPS) to identify the minerals present, to determine the mineral quantities, the liberation of the most important minerals, and the association of the main copper mineral with other minerals in the sample.[1]

The results show that the slow flotation of the chalcopyrite in the samples is due to poor chalcopyrite liberation.

[1]Keywords: Image Analysis, size analysis, liberation.

1 Introduction

On July 20th, 1989 Dr. K.P. Williams of the University of Wales, College of Cardiff submitted several samples, from a typical laboratory copper-rougher flotation test where the copper recovery was less than 70%. The objective was to determine why the copper recovery is low and why the copper is slow floating.

2 Samples

The samples received were:

1. Five-minute concentrate, labelled RCI, ≈3.4 wt % Cu.
2. Next ten-minute concentrate, labelled RCII, ≈0.7 wt % Cu.
3. Tail, labelled RT, ≈0.17 wt % Cu.
4. Concentrate
5. Four samples of -15mm plant feed

The main samples for this study were considered to be the ones corresponding to RCI, RCII, and RT. Polished sections were prepared from each sample, and were studied using a Microprobe SEM-IPS image analysis system (MP-SEM-IPS) coupled with EDS and WDS capabilities.

Careful attention was placed on searching for oxidized copper minerals, since the presence of these could explain the low copper recoveries by flotation.

Image analysis was run to determine mineral quantities, liberation and mineral associations. Image analysis was done using backscattered electron images(BEI). This imaging method relates the contrast and brightness to phase composition. Therefore in black and white images the whitest phase has the highest average atomic number. Grey levels from BEI were used to discriminate between quartz, mica, iron oxides, pyrite, chalcopyrite, and sphalerite. However a copper map (WDS) was used to discriminate tetrahedrite-tennantite from bournonite and galena-boulangerite.

Table 1: Mineral quantities in samples RCI, RCII, and RT.

MINERAL	A36 RCI	A36 RCII	A36 RT
Quartz	0.4	0.3	2.7
Mica	0.1	1.4	4.7
Pyrite	81.2	87.1	77.6
Chalcopyrite	9.6	2.1	0.5
Sphalerite and arsenopyrite	2.6	3.3	5.0
Tetrahedrite and tennantite	0.1	$\approx$0	$\approx$0
Bournonite	1.1	0.2	0.1
Galena and boulangerite	2.5	2.7	1.9
Fe-oxides	2.4	2.9	7.5
Total	100.0	100.0	100.0

3 Results

3.1 Mineral quantities

The minerals identified in the samples are: quartz, dolomite, mica, pyrite, chalcopyrite, sphalerite, arsenopyrite, tetrahedrite, tennantite, bournonite, galena, boulangerite, and iron oxides (hematite, etc.).

Mineral quantities were determined by image analysis in vol. % and converted to wt % (Table 1) using appropriate specific gravities.

Oxidized copper minerals were not found in the samples. The copper bearing minerals in the sample are: chalcopyrite, $CuFeS_2$; tetrahedrite, $(Cu,Fe)_{12}Sb_4S_{13}$; tennantite, $(Cu,Fe)_{12}As_4S_{13}$. Table 1 shows that tetrahedrite and tennantite are present in very small quantities and are largely recovered in the first five minutes. Therefore the problem of slow floating copper is associated with chalcopyrite.

3.2 Liberation

Liberation analyses were performed for pyrite, chalcopyrite, sphalerite, tetrahedrite, tennantite and bournonite in each polished section by determining the percent of the mineral of interest in each particle that bears the mineral. However for simplicity, this section presents only the results for chalcopyrite. Appropriate figures for the other minerals are attached in the appendix.

3.2.1 Liberation of chalcopyrite

Figures 1 to 3 present the liberation data for chalcopyrite. For comparison purposes each of the figures shows three graphs, one for each sample, RCI, RCII, and RT.

Figure 1 plots the percent of chalcopyrite in the polished section (PHAREA) that is in particles which contain a given chalcopyrite percent (PHPERC). The graphs show that nearly all the free chalcopyrite is recovered in the concentrate of the first-five minutes. The amount of free chalcopyrite in the tails (sample RT) is almost nil. By increasing the flotation time, the chalcopyrite pulled to the concentrate is essentially locked.

Similar results are shown in Figure 2, which plots the size of the chalcopyrite grain (GRSIZE) that is in particles with a given chalcopyrite content in percent (PHPERC). These plots are in essence a population distribution with respect of the number of chalcopyrite grains. Figure 2 clearly shows the shift in the distribution of chalcopyrite grains. In the first five minutes of flotation, essentially all the free chalcopyrite grains have been recovered; as flotation continues, the locked chalcopyrite grains are being slowly pulled into the concentrate. In the tails, most of the chalcopyrite grains are shifted to the non-liberated side (Figures 1-c and 2-c). Most of the chalcopyrite grains in the tail are in particles with less than 30% chalcopyrite, and a significant part of the chalcopyrite grains have a size between 10 to 60 μm.

Figure 3 shows the cumulative size distribution of the chalcopyrite grains in samples RCI, RCII, and RT. Figure 3-c indicates that 30% of the chal-

copyrite in the tails is in grains smaller than ≈34 μm (K_{30}). It is interpreted from the data that regrinding the tails to 80% minus K_{30} will free ≈80% of the chalcopyrite. However, in the present case a regrind to 80% minus 34 μm should be assessed carefully since it could lead to problems with fines.

3.3 Association of chalcopyrite with other minerals

The association of chalcopyrite with other minerals in the samples was also studied. Table 2 gives the percent of the chalcopyrite in each sample that is free or that is associated with various minerals. The total amount of chalcopyrite is the sum of columns 2 to 7. The sum of the percent chalcopyrite (base total chalcopyrite) in three-mineral particles (columns 9 to 12) can add to more than the Figure in column 7; this is because the chalcopyrite in each of the three-mineral particle bins could have been measured in three of the four ternary associations as "other".

Table 2 shows that 86% of the chalcopyrite in the tails is locked in particles with three or more minerals. Most of the chalcopyrite in ternary particles is associated with pyrite and sphalerite. This is not surprising considering the massive abundance of pyrite in these samples.

Table 2 also shows that the five minute concentrate recovered most of the free chalcopyrite particles, while in the next ten minutes of flotation most of the binary particles with chalcopyrite and pyrite were recovered. The chalcopyrite left in the tails is mostly in particles with three or more minerals.

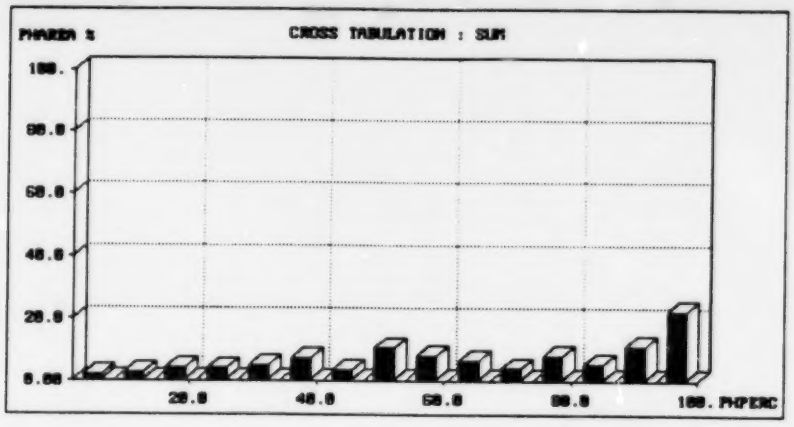

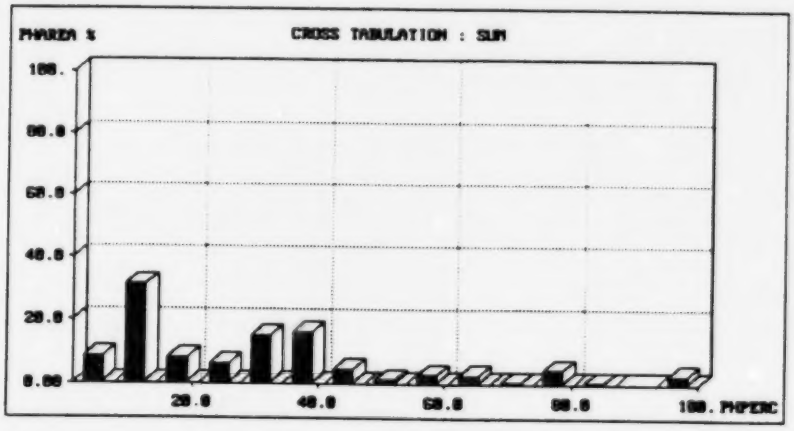

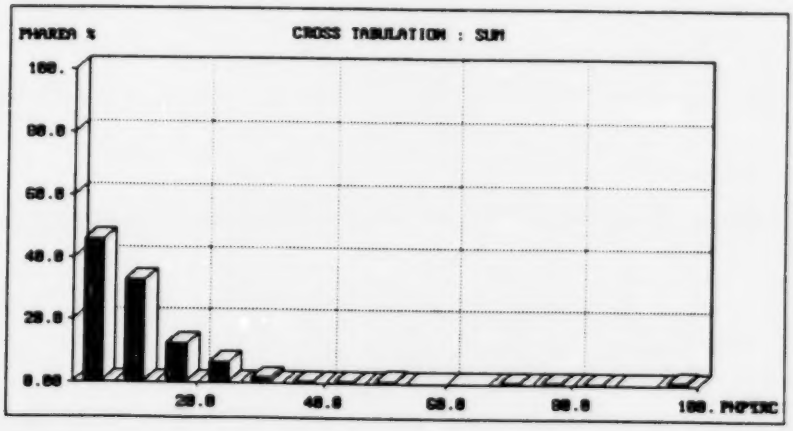

Figure 1: Volumetric percent of chalcopyrite (PHAREA) in each sample that is in particles with a given chalcopyrite percent (PHPERC). Figure 1-a (top) for sample RCI, Figure 1-b (middle) for sample RCII, and Figure 1-c (bottom) for sample RT.

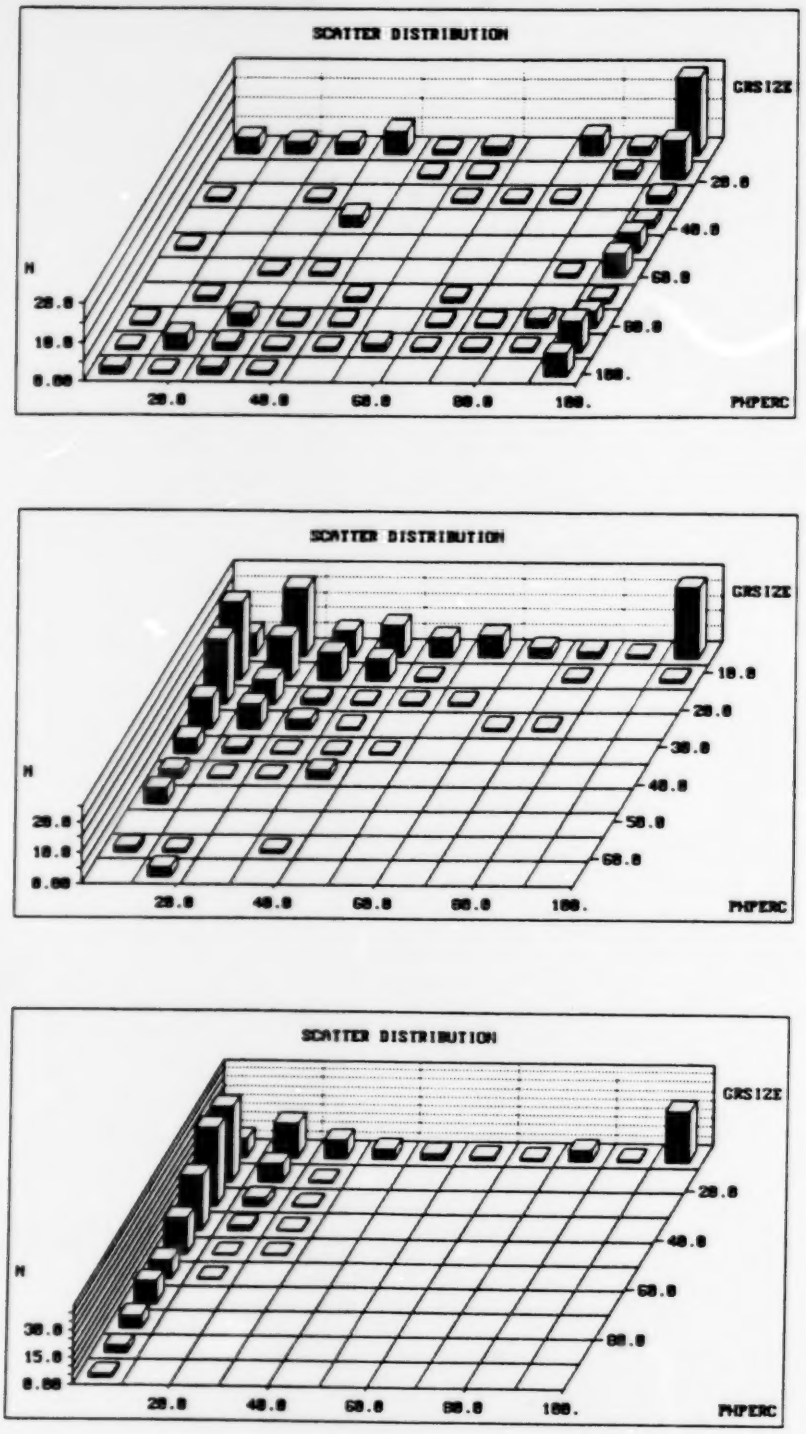

Figure 2: Distribution diagram of the chalcopyrite-bearing particles with respect to the chalcopyrite grain size (GRSIZE) and the particle-volumetric percent of chalcopyrite (PHPERC). Figure 2-a (top) for sample RCI, Figure 2-b (middle) for sample RCII, and Figure 2-c (bottom) for sample RT.

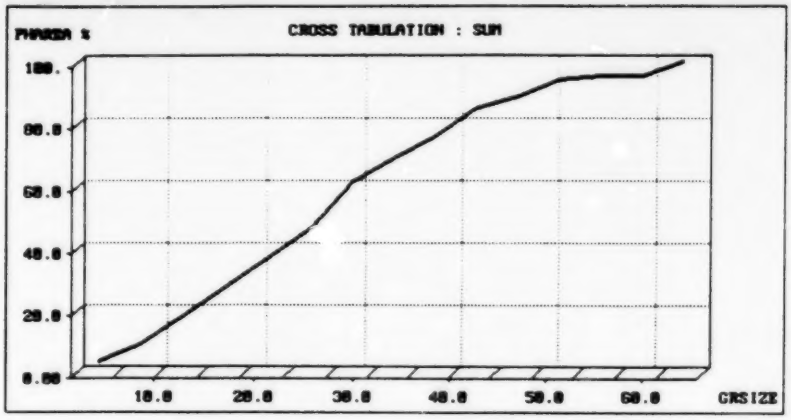

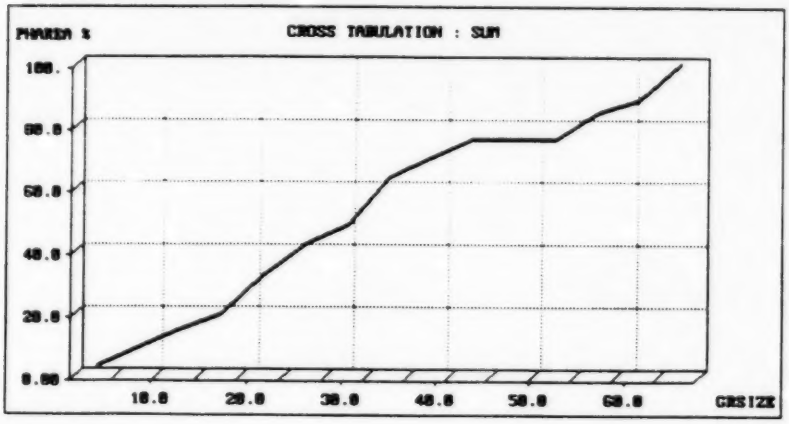

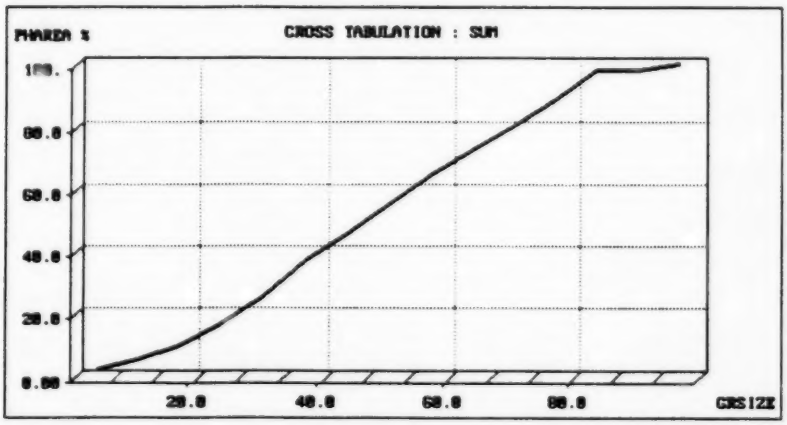

Figure 3: Cumulative size distribution of the chalcopyrite grains. Figure 3-a (top) for sample RCI, Figure 3-b (middle) for sample RCII, and Figure 3-c (bottom) for sample RT.

Table 2: Percent of the total chalcopyrite in each size fraction that is associated in various types of locked particles.

PRODUCT. μm	cp-g	cp-py	cp-sp	cp-tt+ tn+bo	≥80% cp free cp	total cp in ternaries	total cp	cp-g-ot	cp-py-ot	cp-sp-ot	cp-tt+ tn+bo-ot
1	2	3	4	5	6	7	8	9	10	11	12
RCI	0.0	41.0	2.2	0.1	39.8	16.9	100	≈0	15.8	12.2	7.5
RCII	0.0	29.8	6.2	0.1	4.4	59.4	100	21.3	58.7	40.2	11.6
RT	0.0	8.5	3.3	0.0	1.5	86.8	100	32.4	87.7	77.3	7.4

cp= chalcopyrite, g=non-sulphide minerals, py=pyrite, sp=sphalerite, tt=tetrahedrite, tn=tennantite, bo=bournonite, ot=unspecified mineral

4 Conclusions

The slow flotation of the chalcopyrite in these samples is not due to the presence of oxidized copper minerals, but is related to locked chalcopyrite. A regrind of the rougher tails and refloat could improve copper recovery. Attention must be paid to the production of fines and flotation techniques that are more efficient for fine feeds (e.g. columns) should be considered for the flotation of the reground tails.

APPENDIX

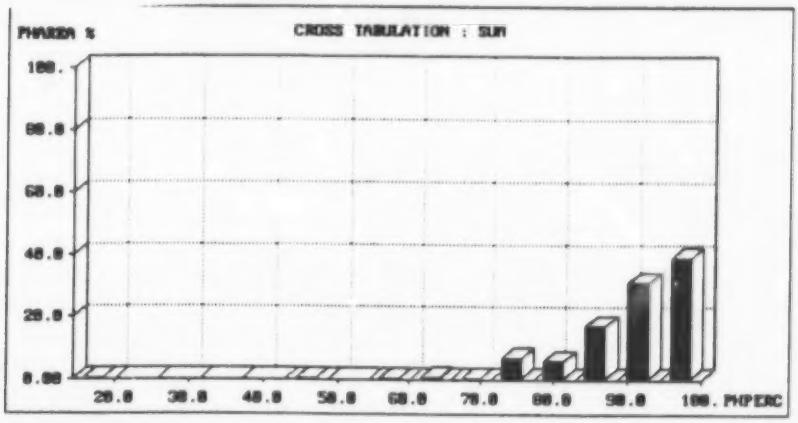

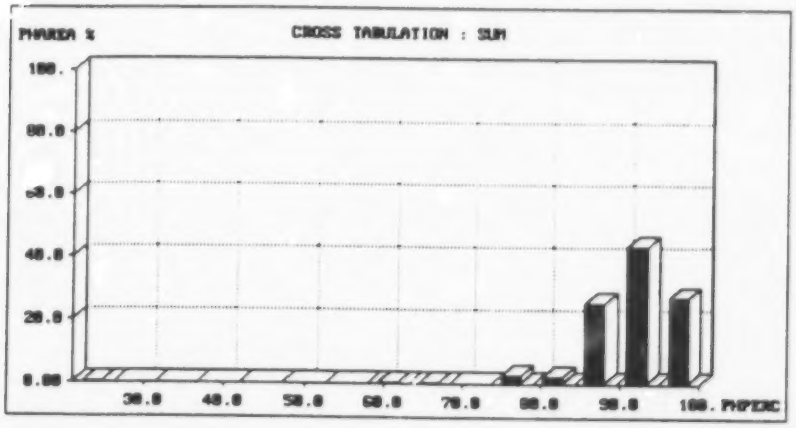

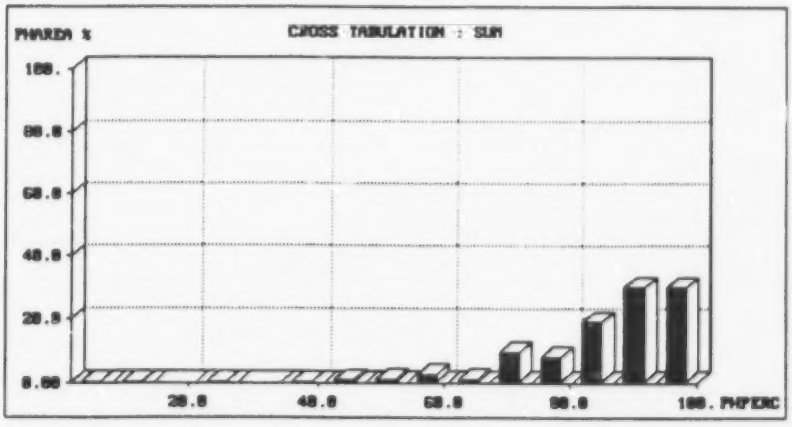

Figure 1: Volumetric percent of pyrite (PHAREA) in each sample that is in particles with a given pyrite percent (PHPERC). Figure 1-a (top) for sample RCI, Figure 1-b (middle) for sample RCII, and Figure 1-c (bottom) for sample RT.

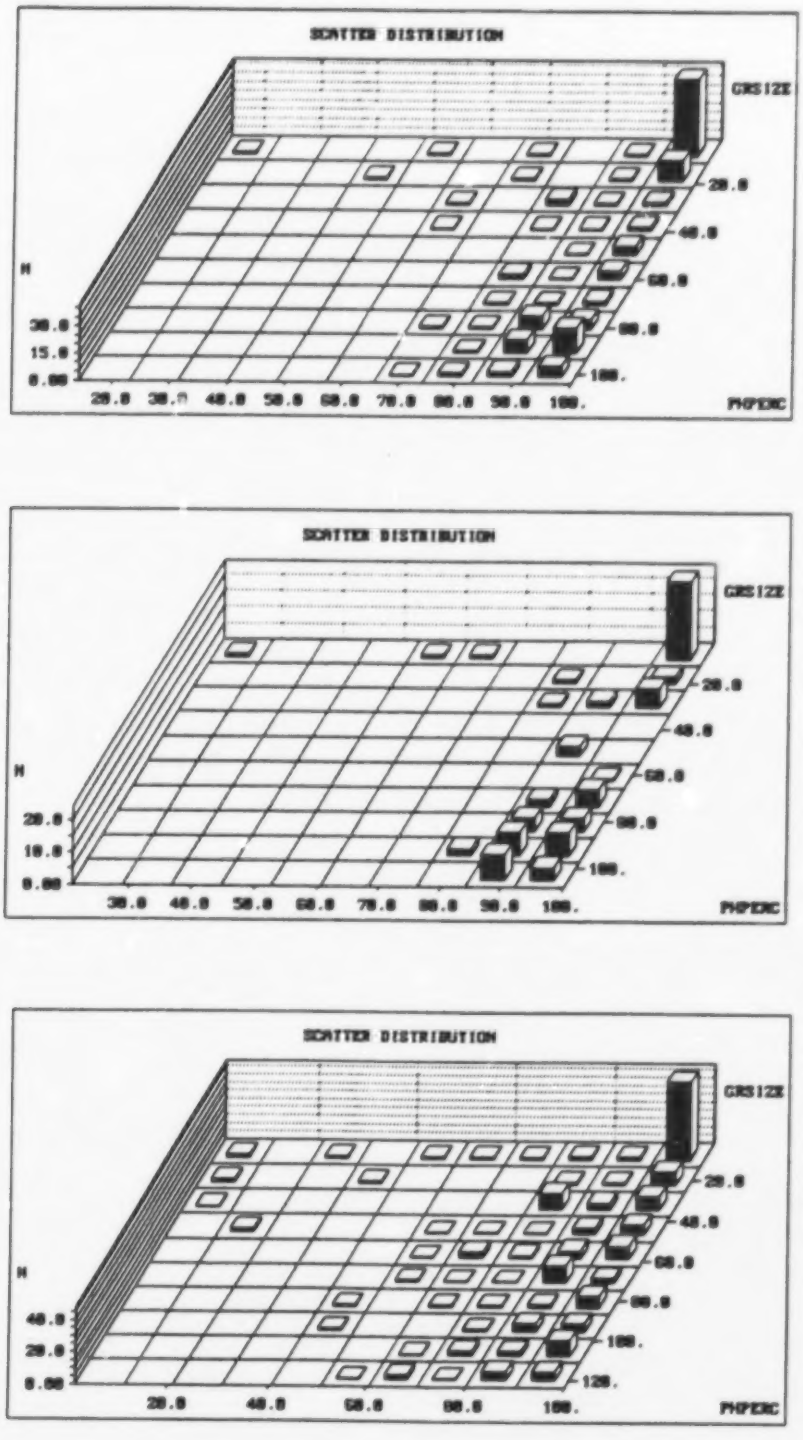

Figure 2: Distribution diagram of the pyrite-bearing particles with respect to the pyrite grain size (GRSIZE) and the particle-volumetric percent of pyrite (PHPERC). Figure 2-a (top) for sample RCI, Figure 2-b (middle) for sample RCII and Figure 2-c (bottom) for sample RT.

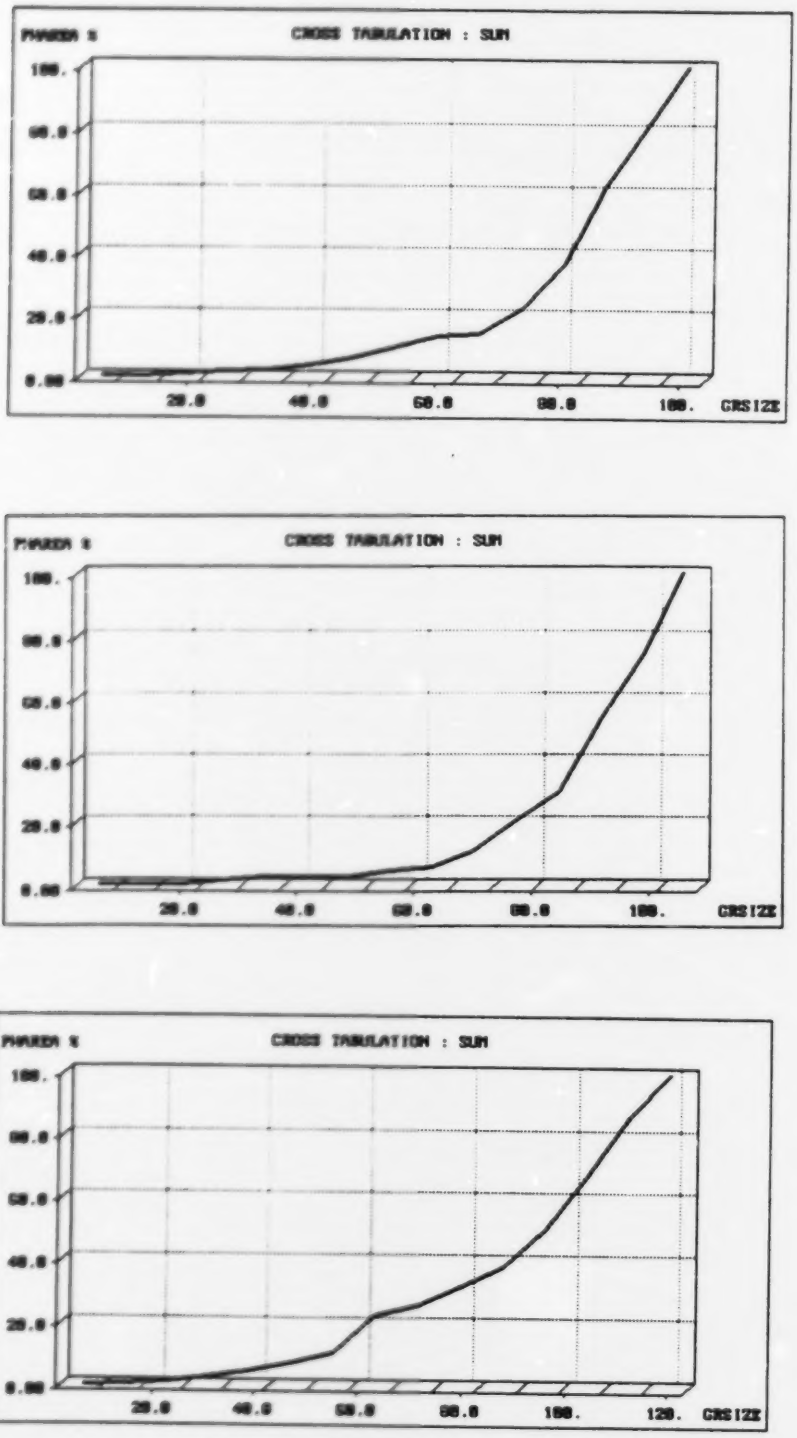

Figure 3: Cumulative size distribution of the pyrite grains. Figure 3-a (top) for sample RCI, Figure 3-b (middle) for sample RCII, and Figure 3-c (bottom) for sample RT.

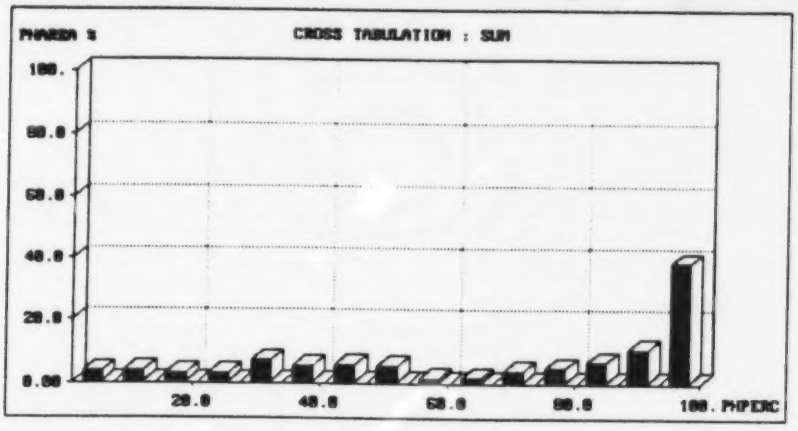

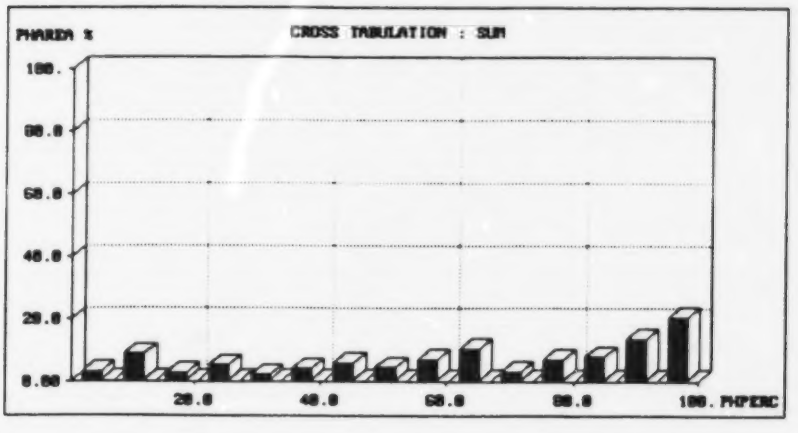

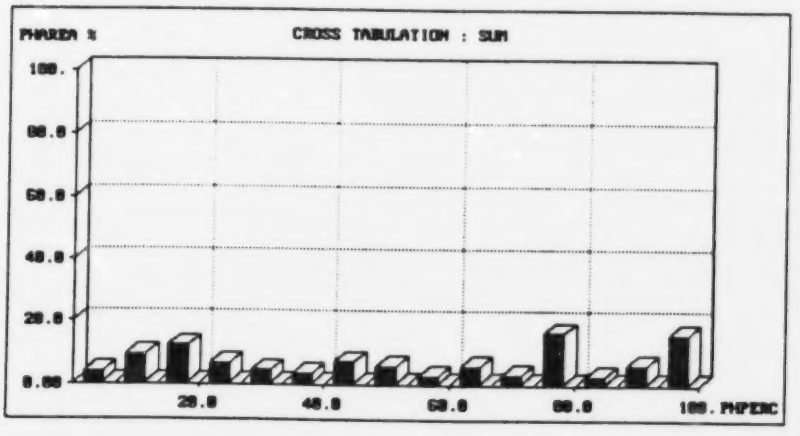

Figure 4: Volumetric percent of sphalerite (PHAREA) in each sample that is in particles with a given sphalerite percent (PHPERC). Figure 4-a (top) for sample RCI, Figure 4-b (middle) for sample RCII, and Figure 4-c (bottom) for sample RT.

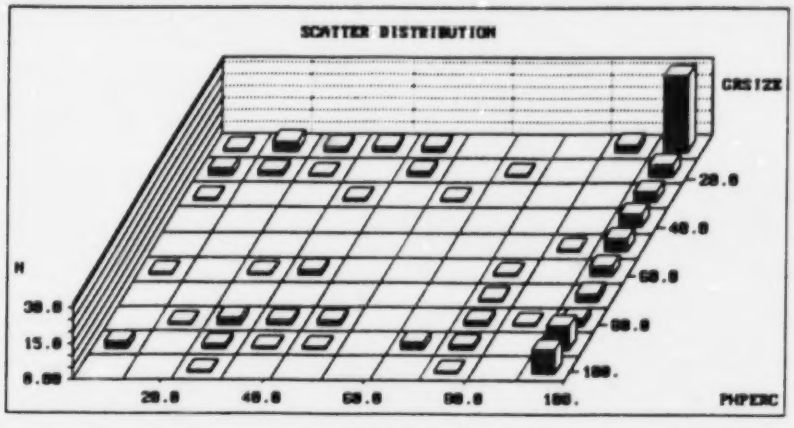

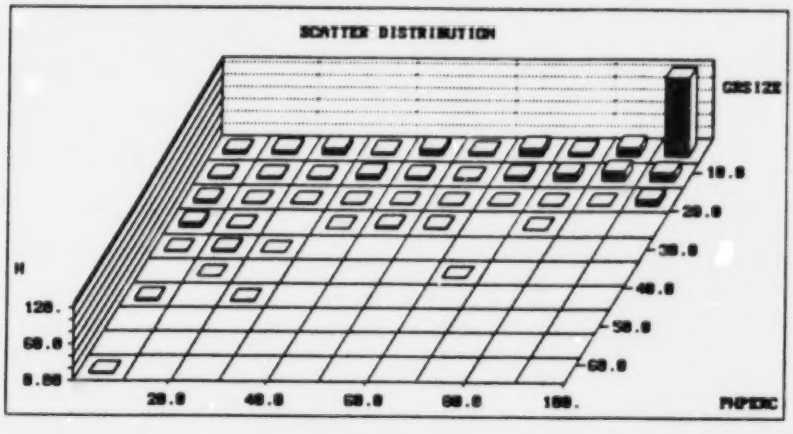

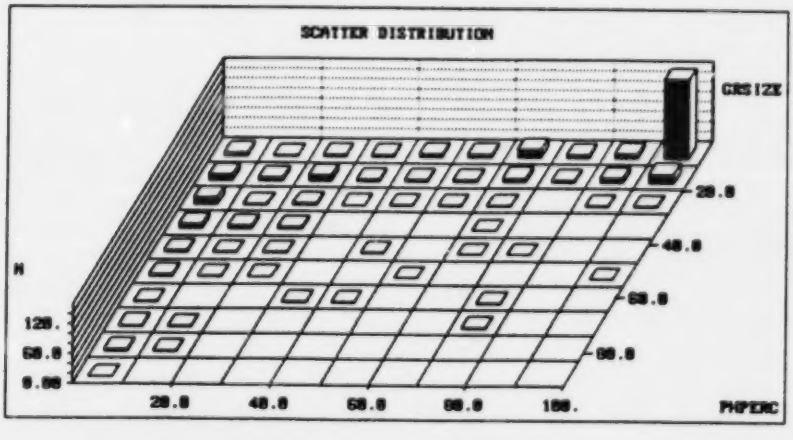

Figure 5: Distribution diagram of the sphalerite-bearing particles with respect to the sphalerite grain size (GRSIZE) and the particle-volumetric percent of sphalerite (PHPERC). Figure 5-a (top) for sample RCI, Figure 5-b (middle) for sample RCII, and Figure 5-c (bottom) for sample RT.

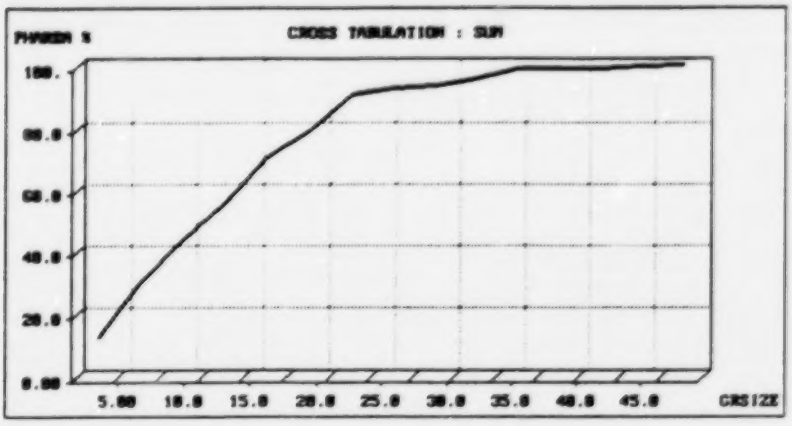

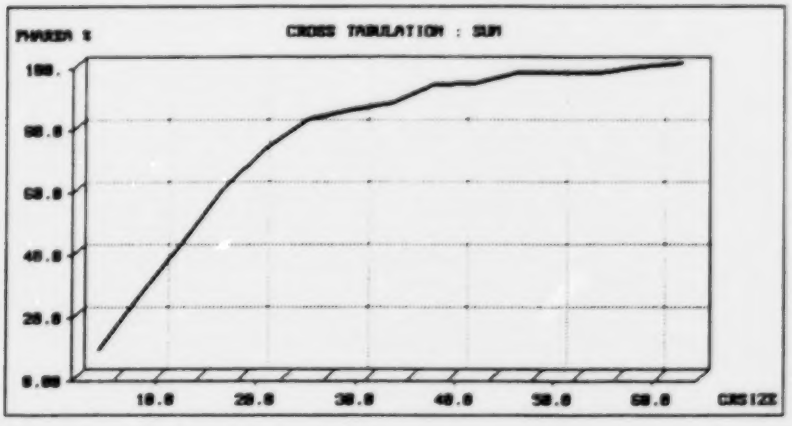

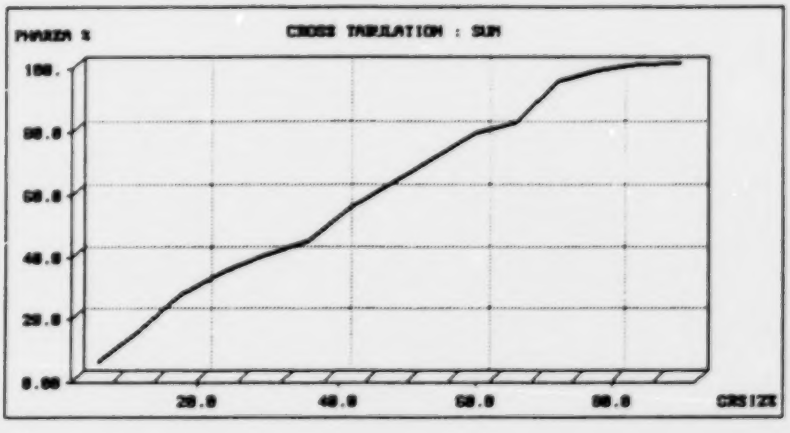

Figure 6: Cumulative size distribution of the sphalerite grains. Figure 6-a (top) for sample RCI, Figure 6-b (middle) for sample RCII, and Figure 6-c (bottom) for sample RT.

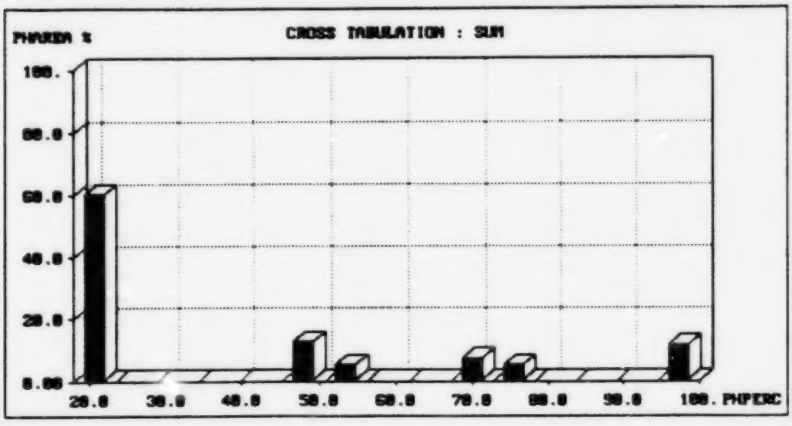

Figure 7: Volumetric percent of tetrahedrite plus tennantite (PHAREA) in each sample that is in particles with a given grain percent (PHPERC). Figure 7-a (top) for sample RCI, Figure 7-b (absent) for sample RCII, and Figure 7-c (absent) for sample RT.

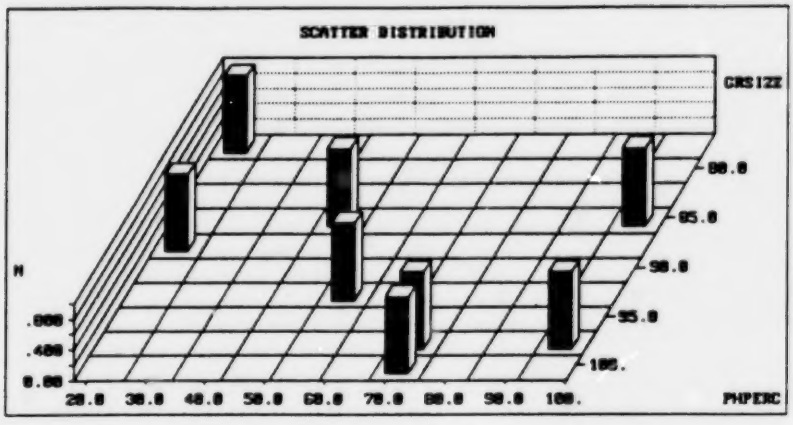

Figure 8: Distribution diagram of the tetrahedrite plus tennantite-bearing particles with respect to their grain size (GRSIZE) and the particle volumetric percent of inclusion (PHPERC). Figure 8-a (top) for sample RCI, Figure 8-b (absent) for sample RCII, and Figure 8-c (absent) for sample RT.

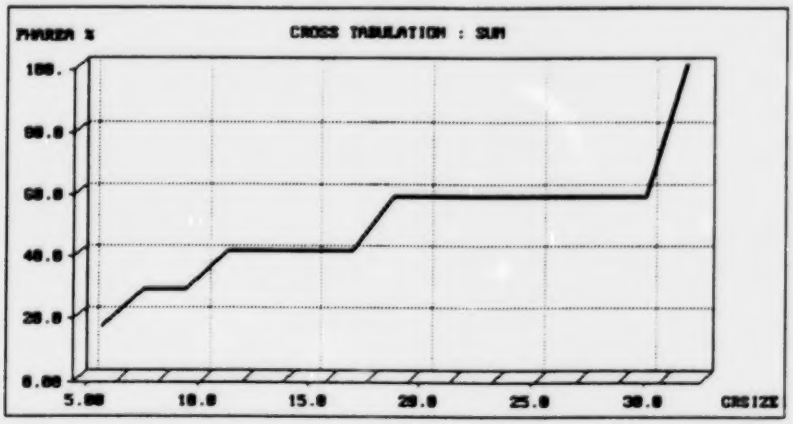

Figure 9: Cumulative size distribution of the tetrahedrite plus tennantite grains. Figure 9-a (top) for sample RCI, Figure 9-b (absent) for sample RCII, and Figure 9-c (absent) for sample RT.

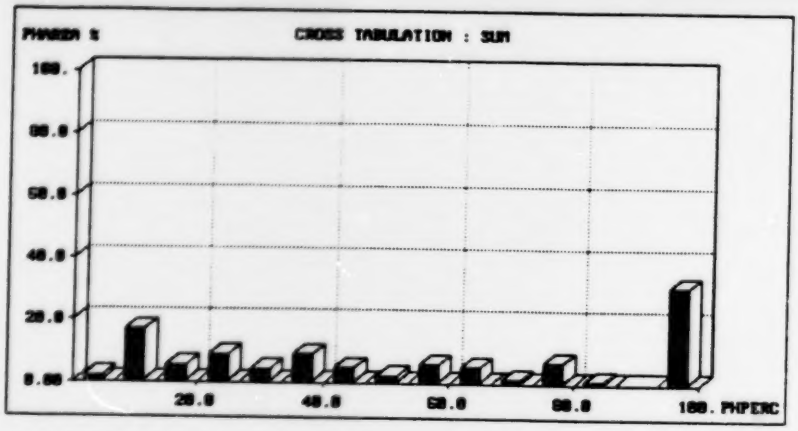

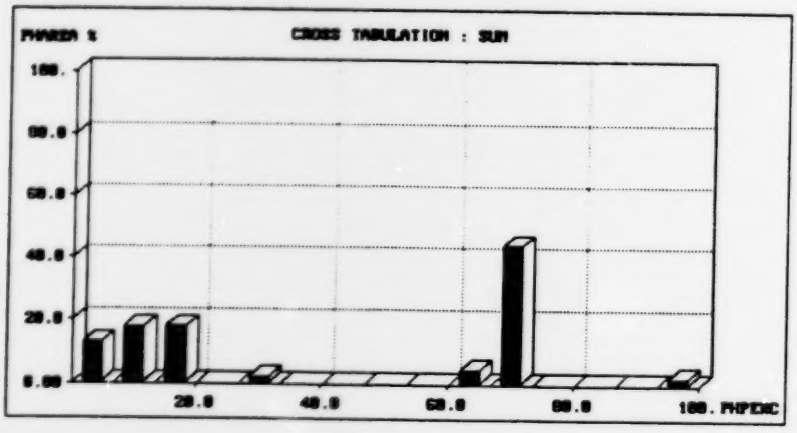

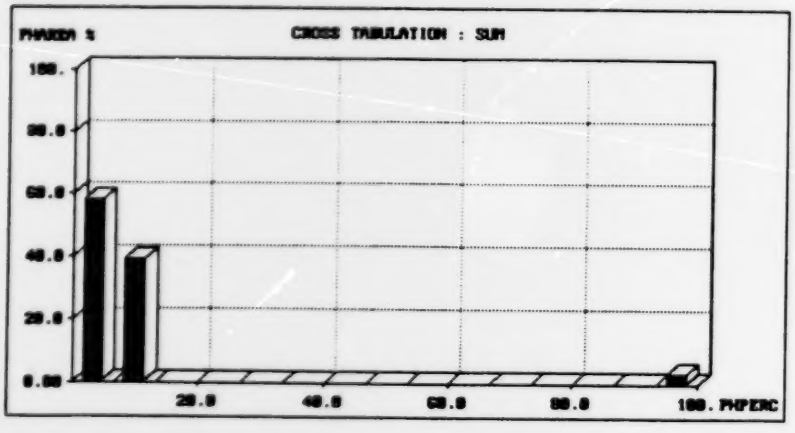

Figure 10: Volumetric percent of bournonite (PHAREA) in each sample that is in particles with a given bournonite percent (PHPERC). Figure 10-a (top) for sample RCI, Figure 10-b (middle) for sample RCII, and Figure 10-c (bottom) for sample RT.

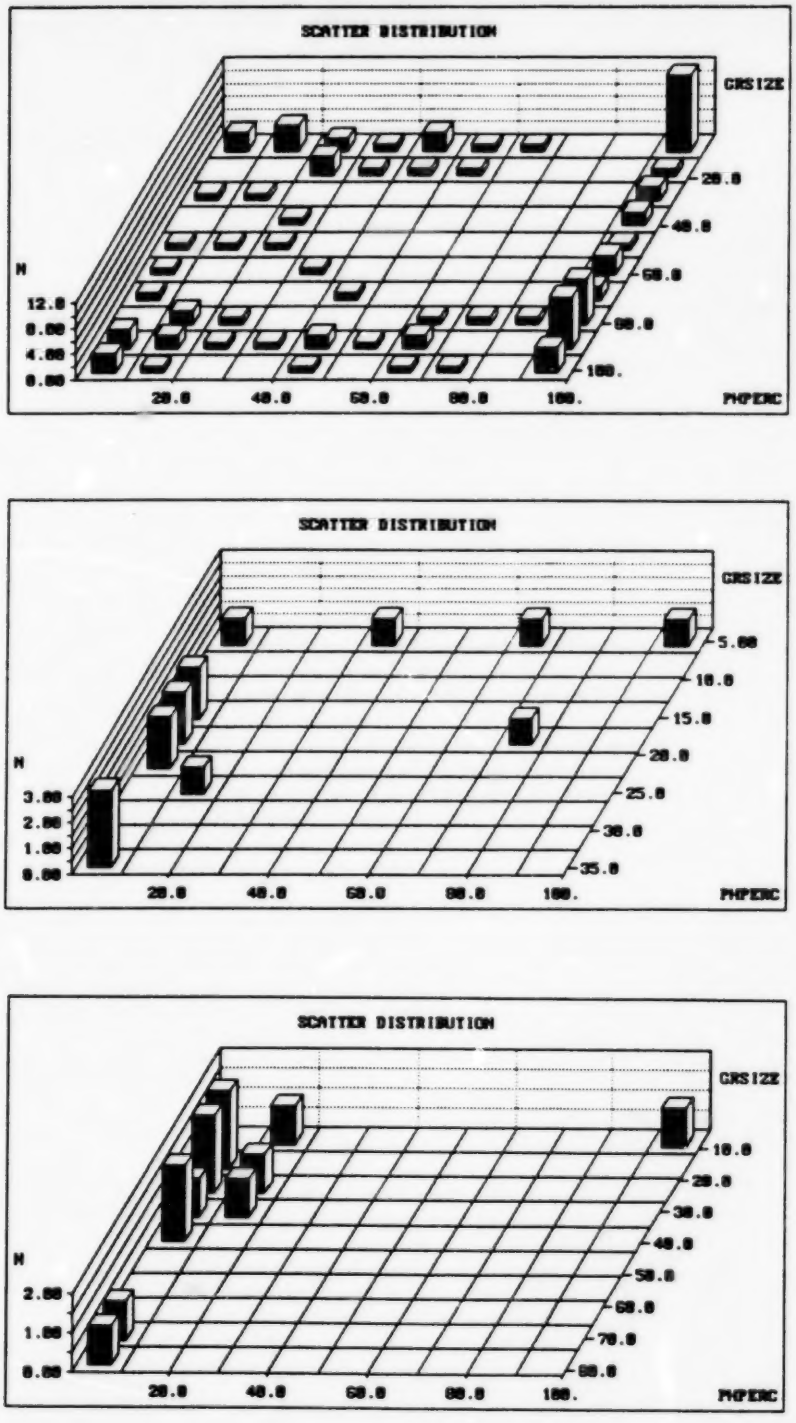

Figure 11: Distribution diagram of the bournonite-bearing particles with respect to grain size (GRSIZE) and the particle-volumetric percent of bournonite (PHPERC). Figure 11-a (top) for sample RCI, Figure 11-b (middle) for sample RCII, and Figure 11-c (bottom) for sample RT.

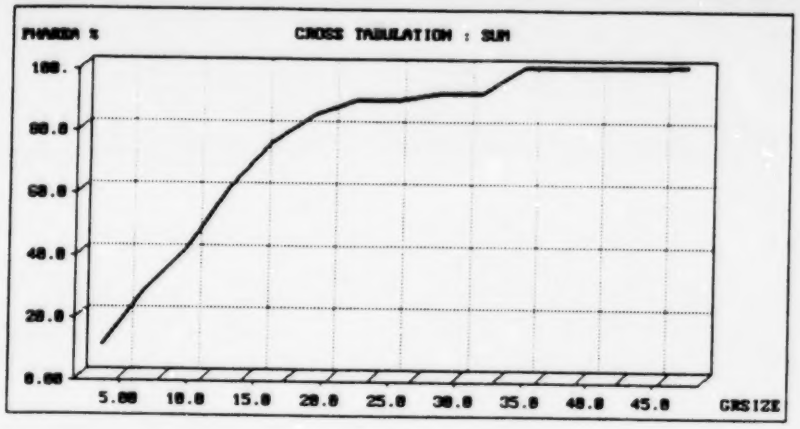

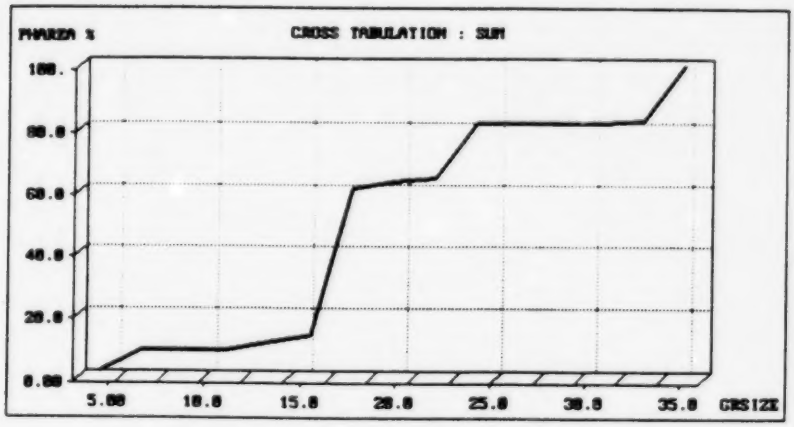

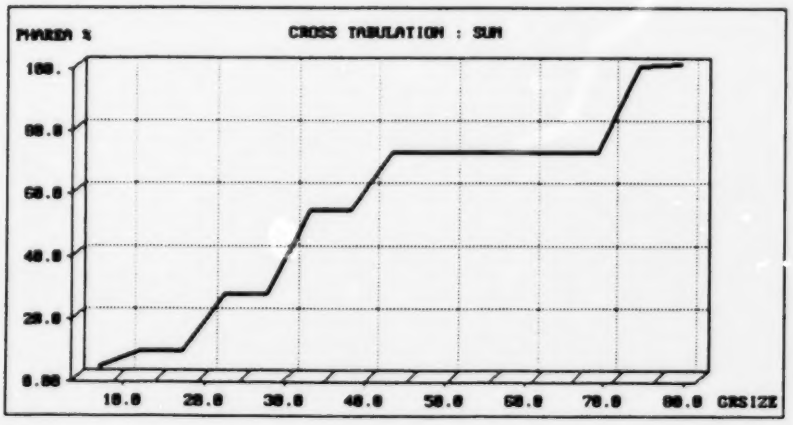

Figure 12: Cumulative size distribution of the bournonite grains. Figure 12-a (top) for sample RCI, Figure 12-b (middle) for sample RCII, and Figure 12-c (bottom) for sample RT.